Toughness Deterioration in Advanced High Strength Bainitic Steels

F.G. Caballero[a], J. Chao[a], J. Cornide[a], C. García-Mateo[a], M.J. Santofimia[b,1] and C. Capdevila[a]

[a] Department of Physical Metallurgy, Spanish National Center for Metallurgical Research (CENIM-CSIC), Avda Gregorio del Amo, 8; Madrid, E-28040, Spain, fgc@cenim.csic.es; jchao@cenim.csic.es; jca@cenim.csic.es; cgm@cenim.csic.es; ccm@cenim.csic.es
[b] Department of Materials Science and Engineering, Delft University of Technology, Mekelweg 2, 2628 CD, Delft, Netherlands, m.santofimianavarro@nimr.nl

Corresponding Author:
F.G. Caballero
Spanish National Center for Metallurgical Research (CENIM-CSIC)
Av. Gregorio del Amo, 8
28040 MADRID
Spain

Tlf: +34 91 553 89 00 (Ext 373)
Fax +34 91 534 7425
E-mail: fgc@cenim.csic.es

Abstract

Carbide free bainitic steels alloyed with manganese have achieved the highest strength and toughness combinations to date for bainitic steels. Ultimate tensile strengths ranging from 1600 to 1800 MPa were achieved while keeping a total elongation higher than 10 %. Their toughness at room temperature matches tempered martensitic steels, known to be the best-in-class regarding this property. This improvement in toughness is achieved suppressing the precipitation of cementite during bainite formation by alloying the steel with about 1.5 wt-% of silicon. However, it has been observed that strongly orientated martensite bands, associated to inhomogeneous manganese redistribution during solidification, leads to a remarkable deterioration in toughness in these advanced bainitic steels. The stress concentration associated with highly heterogeneous hardness distribution in the microstructure contributes to the premature crack nucleation.

Keywords: toughness, coalesced bainite, banding, steel

Introduction

Very early studies by Irvine and Pickering [1] established that conventional bainitic steels are not as successful as quenched and tempered martensitic steels. This is because cementite is brittle and cracks under the influence of the stresses generated by dislocation pile-ups [2]. The crack may then propagate into the bainitic ferrite under appropriate conditions of stress and temperature. However, the precipitation of cementite from austenite during bainite formation can be suppressed by alloying the steel with about 1.5 wt-% of silicon [3-6] since the driving

[1] Instituto Madrileño de Estudios Avanzados en Materiales (IMDEA-Materiales), E. T. S. de Ingeniería de Caminos 28040 Madrid, Spain

force for precipitation is dramatically reduced when the cementite is forced to inherit the silicon present in the parent phase [7].
Bainitic microstructure in high silicon steels consists of fine plates of bainitic ferrite separated by carbon-enriched regions of austenite [8,9]. There may also be some martensite present. This bainitic microstructure has achieved the highest strength and toughness combinations to date for bainitic steels. Ultimate tensile strengths ranging from 1600 to 1800 MPa were achieved while keeping a total elongation higher than 10 %. Their toughness at room temperature matches tempered martensitic steels, known to be the best-in-class regarding this property [10-15].
This improvement in toughness reached in high silicon bainitic steels is attributed to the replacement of brittle interlath cementite of the upper conventional bainite structure by interlath films of softer retained austenite. The enhancement of toughness of ferritic steels by second phase austenite regions to give duplex structures is similar to the approach adopted in the past for more highly alloyed steels [16].
Earlier studies in high silicon bainitic steels [8,9] involving comparative impact toughness measurements showed the desirability of achieving thermal and mechanical stability of austenite by compositional and heat treatment control which results in the retained austenite phase dispersed as thin interlath films rather than in blockier volumes. Blocky austenite is less thermal and mechanically stable, and either form of instability could lead to brittle martensite present in the microstructure which degrades the toughness. In the studied steels, retained austenite is only present as very stable films between the subunits of bainitic ferrite mainly consequence of the high volume fraction of bainitic ferrite achieved. This is a result of the alloy design procedure in which every effort is made to increase the amount of bainitic ferrite so as to consume the blocks of austenite by optimisation of the T_o curve [15].
However, it has been observed a dramatic deterioration of toughness in these carbide free bainitic steels no related to the mechanical stability of austenite. Multiple causes are likely to be responsible of this drop in toughness. For instance, retained austenite is not the only phase imbedded in the bainitic ferrite matrix. Some isolated very fine grains of martensite can be also present in the microstructure. In principle, the presence of a very hard phase, such as martensite, in bainitic microstructure, would be undesired because they could be detrimental to toughness. Other causes such as the presence of martensite bands in the microstructure [17,18] and the coalescence of bainite platelets [19] are also examined as possible explanations for the deterioration of the impact energy of advanced high strength bainitic steels.

Materials and Experimental Procedure

Chemical compositions of the studied bainitic steels are listed in Table 1. Alloys were manufactured by ArcelorMittal (Maizières les Metz-France) as 180x80x12 mm^3 plates. All laboratory heats were elaborated in a 60 kg vacuum induction furnace under inert atmosphere. The generator power was 80 kW. Pure (>99.9 %) electrolytic iron and addition of the alloying elements one after each other were used. Carbon deoxidation was performed and an analysis of C, S, N, O was made on line during elaboration for the final adjustment of composition. Samples were hot rolled from 40 to 12 mm in several passes finishing at temperatures ranging from 900 to 930ºC. The desired bainitic microstructure was obtained in all the steels by air cooling from ~500ºC after an initial accelerating cooling.
Specimens, longitudinal and transverse to the hot rolling direction, were ground and polished using standardised techniques for metallographic examination. A 2 % Nital etching solution was used to reveal bainitic microstructure by light optical microscopy (LOM) and scanning

electron microscopy (SEM) in a JEOL JSM-6500F field emission gun scanning electron microscope operating at 7 kV.

The volume fraction of martensite in bands, $V_{M\ in\ bands}$, was determined by a systematic manual point counting procedure in LOM micrographs at low magnification (X100), whereas the volume fraction of martensite/austenite (M/A) constituent inside bainite sheaves was estimated by the same procedure on SEM micrographs at a magnification of X1500.

Quantitative X-ray diffraction analysis was used to determine the fraction of retained austenite and its carbon content. For this purpose, 11x5x2 mm^3 samples were machined. After grinding and final polishing using 1 μm diamond paste, the samples were lightly etched to obtain an undeformed surface. They were then step-scanned in a SIEMENS D 5000 X-ray diffractometer using unfiltered Cu K_α radiation. The scanning speed (2θ) was less than 0.3 degree/min. The machine was operated at 40 kV and 30 mA. The volume fraction of retained austenite was calculated from the integrated intensities of (200), (220) and (311) austenite peaks, and those of (002), (112) and (022) planes of ferrite. Moreover, retained austenite composition was calculated making use of the relationship between lattice parameter and chemical composition as reported in ref. [20] and assuming that during transformation only carbon diffuses. Thus, the concentration ratios of all elements but carbon should be equal in the bulk material as in the retained austenite [21].

Specimens for transmission electron microscopy (TEM) were machined down to 3 mm diameter rods. The rods were sliced into 400 μm thick discs and subsequently ground down to foils of 50 μm in thickness on wet 1200 grit silicon carbide paper. These foils were finally electropolished at room temperature until perforation occurred, using a twin-jet electropolisher set at a voltage of 40 V. The electrolyte consisted of 5 % perchloric acid, 15 % glycerol and 80 % methanol. The foils were examined in a JEOL JEM 2010 transmission electron microscope at an operating voltage of 200 kV.

The Standard Practice ASTM E 1268-99 for "Assessing the Degree of Banding or Orientation of Microstructures" proposes the characterisation of the degree of banding in the microstructure by the anisotropy index, *AI*, and the mean edge-to-edge spacing of the bands, λ, which rely on simple stereological methods. The anisotropy AI is estimated from the following equation,

$$AI = \overline{N}_{L\perp} / \overline{N}_{L\parallel} \qquad (1)$$

where $\overline{N}_{L\perp}$ is the mean number of feature interceptions with test lines perpendicular to the deformation direction per unit length of the test lines, and $\overline{N}_{L\parallel}$ is the mean number of feature interceptions with test lines parallel to the deformation direction per unit length of the test lines. For a randomly oriented, non-banded microstructure, *AI* has a value of one. As the degree of orientation or banding increases, the anisotropy index increases.

The mean free path spacing, λ, is determined as follows,

$$\lambda = (1 - V_V) / \overline{N}_{L\perp} \qquad (2)$$

where V_V is the volume fraction of the banded or the oriented phase, $V_{M\ in\ bands}$ in the present work. Both parameters, AI and λ have been manually determined in longitudinal samples using low magnification micrographs (X50).

Transversal tensile specimens with a section of 3 mm diameter and a gauge length of 19 mm were tested at room temperature using a Microtest EM2/100/FR testing machine fitted with a 100 kN load cell. A deformation rate of 6 x 10^{-4} s^{-1} was used in all the experiments.

Transversal impact toughness was measured on normalized Charpy V-notched (10x10 mm²) samples at temperatures between -40ºC and 150ºC using a 300 J Charpy testing machine. Specimens were tested in accordance with the steel standard BS EN 10 045-1: 1990. Six specimens were tested at each temperature for every alloy.
Vickers hardness HV30 tests results are quoted here as an average of at least five individual measurements. Moreover, micro Vickers hardness measurements (0.2 kg-1960 mN) were performed. The indentation microhardness was confined to a region of ~56400 μm^2 (indentation site ~25 μm and the distance between adjacent indentations ~100 μm) including several martensite bands and bainite sheaves of the microstructure.

Results and Discussion

Microstructure of Advanced Bainitic Steels containing manganese

Microstructural characterisation at low magnification reveals that all the samples have a microstructure consisting of bainite sheaves and bands of martensite (see lighter etched regions in optical micrographs of Fig. 1). Microstructural banding is due to the segregation of substitutional alloying elements during dendritic solidification. Several investigations have shown that manganese is the alloying element most likely to be responsible for the development of microstructural banding in low alloy steels [17,22,23]. Thompson and Howell [24] investigated banding in 0.15 wt-%C, 1.40 wt-%Mn steel and concluded that increasing the cooling rate from the austenitic condition reduces the intensity of banding because it reduces the Ar_3 temperature differences of the segregated bands. However, in the present work, the cooling rate during hot rolling simulation has not been fast enough to avoid the presence of banding in the final microstructure.

(FIGURE 1)

Bainite sheaves are examined in detail using SEM micrographs (see Fig. 2). Bainite is formed by thin and long parallel bainitic ferrite plates and martensite/austenite (M/A) constituents. In general, SEM micrographs illustrate the extraordinary small size of the M/A grains inside bainite sheaves.

((FIGURE 2)

In discussing the morphology of the austenite remaining after partial transformation to bainite, it is necessary to distinguish between the blocky morphology of austenite located between the sheaves of bainite and the films of austenite which are retained between the subunits within a given sheaf of bainite. Film and blocky austenite fractions can be deduced from the total fraction of retained austenite determined by X-ray analysis following Bhadeshia and Edmonds equations [4]. In the present work, retained austenite is only present as films between the subunits of bainitic ferrite because of the high volume fraction of bainitic ferrite. Finally, the difference between the volume fraction of M/A constituent and the volume fraction of austenite films corresponds to the martensite fraction inside bainite sheaves, $V_{M\ in\ bainite}$. Quantitative experimental data on this advanced bainitic microstructure are presented in Table 2.
The amount of residual austenite just after bainite formation is given by (1- $V_{\alpha b}$). The fraction of this quantity, which may decompose partially to martensite during subsequent cooling to

ambient temperature, is related to the carbon content in austenite, x_γ, determined by X-ray diffraction. It follows that the thermal stability of the residual austenite is higher for higher carbon content. In this sense, certain inconsistency could have been detected for the carbon content of retained austenite among the steels. For instance, CENIM 3 exhibits the lowest overall martensite content in the microstructure, whereas CENIM 6 shows much higher martensite fraction despite the higher carbon content in austenite. This must be a consequence of the fact that the isolated films of austenite between the bainite plates can accumulate a significant amount of carbon [25]. Moreover, we should bear in mind that X-ray analysis carbon content estimation is an average of a larger volume that may contain any carbon enriched regions such as dislocations and phase interfaces, characteristic features of this type of microstructure [26].

Bright-field images in Fig. 3 confirm that the microstructure in both steels consists of carbide-free upper bainite with interlath retained austenite films. These films have sometimes a typical wavy morphology characteristic of the bainite in high-silicon steels.

((FIGURE 3)

Strength and Toughness of Advanced Bainitic Steels

Tensile test results are listed in Table 3 for all the alloys. Plates of bainitic ferrite are typically 10 μm in length and about 0.2 μm in thickness [15, 27] giving a rather small mean free path for dislocation glide. The main microstructural contribution to the strength of bainite is from the extremely fine grain size of bainitic ferrite. It is difficult to separate the effect of retained austenite on strength in these steels from other factors. Qualitatively, austenite can affect the strength in several ways; residual austenite can transform to martensite during cooling to room temperature, thus increasing the strength. On the other hand, retained austenite interlath films can increase the strength by transforming to martensite during testing, similar to the behaviour of TRIP steels.

Charpy impact test results are also listed in Table 3. High toughness values in these advanced bainitic steels are attributed to the replacement of brittle interlath cementite of the upper conventional bainite structure by very stable interlath films of softer retained austenite. Results demonstrate that the common belief that the toughness of high strength steels can be improved by adding nickel is not justified. It is found that nickel addition in CENIM 4 steel did not lead to an improvement in the impact toughness in these bainitic steels containing manganese. This is consistent with results reported elsewhere for strong steel weld metals [28].

As Fig. 4 suggested, the relation between the impact energy and the phase fractions is not significant. However, the optimum combination of strength and toughness in these steels is directly related to the high volume fraction of bainite reached in the microstructure. The results are consistent with the enhancement of toughness expected when the presence of unstable blocky austenite is avoided and the amount of martensite is reduced (See Fig. 4.b), in general, when the thermal and mechanical stability of residual austenite is increased.

However, results shown in Table 2 and Fig. 4 indicate a dramatic deterioration of toughness in CENIM 6 steel (see open symbol in Fig. 4) no related to the mechanical stability of austenite. As mentioned above, in all the studied steels, retained austenite is present as high stable films between the subunits of bainitic ferrite.

((FIGURE 4)

Possible Explanations for the Deterioration of Toughness

Multiple causes are likely to be responsible of this drop in toughness. For instance, the presence of a hard phase, such as martensite, in a bainitic microstructure, would be undesired because they could be detrimental to toughness. Figure 5 shows Charpy impact results as a function of the volume fraction of martensite in bands and inside bainite sheaves. The tendency of the martensite to crack in a mixture of austenite and martensite depends on its absolute size. Chatterjee and Bhadeshia [29] demonstrated that in these mixtures, it is more difficult to crack fine martensite. Thus, martensite islands, with a smaller size than the distance between cracks on single martensite plates determined to be 10 μm [29], do not readily crack causing brittle behaviour. SEM micrographs in Fig. 2 illustrate the extraordinary small size of the martensite grains inside bainite sheaves. Therefore, only martensite in bands could be the responsible for brittle behaviour. However, the amount or size of the martensite grains observed in CENIM 6 microstructure can not explain the deterioration of toughness observed in this steel.

((FIGURE 5)

Other causes such as the coalescence of bainite platelets and the presence of martensite bands in the microstructure are examined below as possible explanations for the deterioration of the impact energy of advanced high strength bainitic steels.

Coalesced bainite.- Recent experiments in steel weld metals have confirmed that coalescence of bainite leads to a dramatic deterioration in toughness [28,19]. Coalesced bainite occurs when adjacent small platelets of bainite, i.e. sub-units, merge to form a single larger plate. This leads to a markedly bimodal distribution of plate thicknesses, with the fine plates about 0.2 μm thick and the larger plates ~2-3 μm thick. SEM micrographs in Fig. 6 shows evidence of coalescence process in two of the studied alloys. Bimodal distribution of plate sizes is clear in these bainitic microstructures.

((FIGURE 6)

TEM micrographs in Fig.7 show higher resolution images of coalesced bainite in which a sheaf of bainite initiating as many identically oriented platelets of an austenite grain boundary, with each platelet separated by a retained austenite film. The platelets later merge into a single coarse crystal. The films of austenite disappear along the length of the sheaf, resulting in a homogeneous plate, and the excess carbon in the bainitic ferrite precipitates within the ferrite as cementite, as Fig. 7 illustrates. It is particularly noticeable in Fig. 7b that there is a precipitate free zone at its borders. This is because only the carbon near the interface with the austenite can partition once coalescence begins, whereas that remote from the interface must precipitate [30].

((FIGURE 7)

The question then arises as to why bainite has coalesced in CENIM 5 and 6. It has been reported [19] that the coalesced bainite form at large driving forces since there must be an adequate driving force for its occurrence in order to sustain the greater strain energy associated with the coarse plate. Calculations on driving force for bainite formation in the studied steels are listed in Table 4. According to these values, CENIM 3 together with CENIM 5 and 6 could exhibit coalesced bainite based on their high driving force values.

However a large driving force is not the only necessary condition for coalesced bainite formation. A large prior austenite grain size must also assist the process of coalescence [19] since the lengthening of sub-units must be allowed to proceed without hindrance. Unfortunately, data on the prior austenite grain size at the finishing rolling temperature of the studied steels are not available.
Electron back scattering diffraction of coalesced bainite [31] confirmed that bainitic platelets that coalesce have an identical crystallographic orientation and hence create a large region without crystallographic discontinuities, thereby reducing the ability to deflect the propagation of cleavage cracks. Coarse scale of coalesced bainite could explain the deterioration of impact toughness detected in CENIM 6 steel. However, the presence of coalesced bainite in the microstructure of CENIM 5 steel does not seem to be detrimental to the impact toughness. There is not clear evidence that the coalescence process essentially affect toughness in these high strength bainitic steels. Results indicate that only the presence of coalesced bainite cannot explain the deterioration of toughness observed in this steel.

Microstructural Banding.- Micro Vickers hardness measurements (0.2 kg-1960 mN) were performed in CENIM 3 and 6 steels (samples with the higher and the lowest impact energy at room temperature, respectively-see Table 3). The indentation microhardness is confined to a region that includes several martensite bands and bainite sheaves of the microstructure (see corresponding micrographs in Figs. 1.c and f). The highest hardness values in Fig. 8 for both steels correspond to the martensite bands in the microstructure (~6.2 GPa in CENIM 3 and ~6.7 GPa in CENIM6). Moreover, bainite matrix seems to be harder in CENIM 6 than in CENIM 3 steel. Precipitation inside coalesced bainite, evident in TEM micrographs of Fig. 7, will explain the very high strength achieved in this steel (Table 3). Bearing in mind that the difference in the martensite content in bands of the two steels is not significant (in the range of standard deviation), histograms reveal a more heterogeneous hardness distribution in CENIM 6 steel related to martensite banding. The stress concentration associated with highly heterogeneous hardness distribution in the microstructure is considered as a possible factor contributing to the premature crack nucleation.

((FIGURE 8)

AI values in Table 5 characterise the degree of martensite banding on longitudinal sections. Microstructures with martensite phase nearly randomly distributed in the bainitic matrix present *AI* values close to one. By contrast, steels with high AI values exhibit strongly orientated martensite bands in the microstructure. On the other hand, λ values give us an idea of the distance between those bands. Results clearly indicate that CENIM 6 steel exhibits a severe banding problem that explains the deterioration of toughness detected in this steel.

Fractographic Analysis.- SEM micrographs of the fracture surface of CENIM 6 steel transversal impact specimen at -40 ºC are shown in Fig. 9. Fractograph of a region close to notch (zone A-Fig. 9c) exhibits some transgranular facets with a facet size of approximately 10 μm, of the order of the martensite band width (see Fig. 1). These regions were observed within a predominantly quasi-cleavage-type fracture surface. At a region far from the crack initiation site but still in the vicinity of the notch (zone B-Fig. 9d), dimpled areas can be seen sporadically within the quasi-cleavage fracture.

((FIGURE 9)

Although it was possible to identify initiation sites by tracing river lines to an origin on low magnification micrographs (Fig. 9b), the initiation site itself was usually featureless (see Fig. 9c). However, results suggested that the boundaries between martensite bands and bainite matrix are the microstructural feature responsible for crack nucleation

Results are consistent with recently reported work [32] where the effect of martensite morphology and distribution in a ferrite matrix on the mechanical properties and the damage accumulation in uniaxial tension was investigated in two different automotive-grade dual phase DP600 steels. SEM analysis of microstructure and damage accumulation revealed that voids nucleation occurs by martensite cracking, separation of adjacent martensite regions, or by decohesion at the ferrite/martensite interface. Martensite morphology and distribution had a significant influence in the accumulation of damage. The steel with a more uniform distribution of martensite showed a slower rate of damage growth and a continuous void nucleation during the deformation process, which resulted in a higher void density before fracture. On the other hand, the steel with a centre-line of martensite through the sheet thickness exhibited accelerated void growth and catastrophic coalescence in the transverse orientation to the applied load.

To avoid or reduce the problem of microstructural banding, it is proposed to modify the hot rolling parameters so the formation of microstructural banding is avoided. Based on former experience [33], the use of higher cooling rates or low coiling temperatures after accelerating cooling is recommended.

Conclusions

Carbide free bainitic steels alloyed with manganese have achieved the highest strength and toughness combinations to date in as-rolled conditions. This improvement in toughness reached is attributed to the replacement of brittle interlath cementite of the upper conventional bainite structure by very stable interlath films of softer retained austenite. However, it has been observed that a high degree of microstructural banding, as a result of an intense segregation of manganese during dendritic solidification, leads to a dramatic deterioration in toughness in these advanced bainitic steels. The stress concentration associated with highly heterogeneous hardness distribution in the microstructure is considered as a possible factor contributing to the premature crack nucleation.

Acknowledgements

The authors gratefully acknowledge the support of the Research Fund for Coal and Steel and the Spanish Ministry of Science and Innovation for funding this research under the contracts RFSR-CT-2008-00021 and MAT2007 – 63873, respectively. All of us want to thank to T. Iung and S. Allain from ArcelorMittal (Maizières les Metz-France) for manufacturing the studied steels.

References

[1] K.J. Irvine, F.B. Pickering, J. Iron Steel Inst. 201 (1963) 518-531.

[2] G.T. Hahn, B.L. Averbach, W.S. Owen, M. Cohen, in: B.L. Averbach, D.K. Felbeck, G.T. Hahn, D.A. Thomas (Eds.), Proceedings of Swampscott Conference on Fracture, Wiley, New York, 1959, pp. 91-114.

[3] S.J. Matas, R.F. Hehemann, Trans. Met. Soc. AIME 221 (1961) 179-185.
[4] R. Entin, in: V. F. Zackay, H.I. Aaronson (Eds.), Decomposition of Austenite by Diffusional Processes, Interscience, New York, 1962, pp. 295-311.
[5] R.F. Hehemann, Phase Transformations, American Society for Metals, Metals Park, Ohio, 1970.
[6] R. Lehouillier, G. Begin, A. Dube, Metall. Trans. 2A (1971) 2645-2653.
[7] E. Kozeschnik, H.K.D.H. Bhadeshia, Mater. Sci. Technol. 24 (2008) 343-347.
[8] H.K.D.H. Bhadeshia, D.V. Edmonds, Metal Sci. 17 (1983) 411-419.
[9] H.K.D.H. Bhadeshia, D.V. Edmonds, Metal Sci. 17 (1983) 420-425.
[10] V.T.T. Miihkinen, D.V. Edmonds, Mater. Sci. Technol. 3 (1987) 422-431.
[11] V.T.T. Miihkinen, D.V. Edmonds, Mater. Sci. Technol. 3 (1987) 432-440.
[12] V.T.T. Miihkinen, D.V. Edmonds, Mater. Sci. Technol. 3 (1987) 441-449.
[13] F.G. Caballero, H.K.D.H. Bhadeshia, K.J.A. Mawella, D.G. Jones, P. Brown, Mater. Sci. Technol. 17 (2001) 512-516.
[14] F.G. Caballero, H.K.D.H. Bhadeshia, K.J.A. Mawella, D.G. Jones, P. Brown, Mater. Sci. Technol. 17 (2001) 517-522.
[15] F.G. Caballero, M.J. Santofimia, C. Capdevila, C. García-Mateo, C. García de Andrés, ISIJ Int. 46 (2006) 1479-1488.
[16] C.W. Marschall, R.F. Hehemann, A.R. Troyano, Trans. ASM 55 (1962) 135-152.
[17] R.A. Grange, Metall. Trans. 2 (1971) 417-426.
[18] A. Sakir Bor, ISIJ Int. 31 (1991) 1445-1446.
[19] H.K.D.H. Bhadeshia, E. Keehan, L. Karlssonz, H.O. Andrén, Trans. Indian Inst. Met. 59 (2006) 689-694.
[20] D.J. Dyson, B. Holmes, J. Iron Steel Inst. 208 (1970) 469-474.
[21] C. Garcia-Mateo, F.G. Caballero, Mater. Trans. 46 (2005) 1839-1846.
[22] V Faccenda, M Falco, C Modena, Metall. Ital. 65 (1973) 133-140.
[23] R Grossterlinden, R Kawalla U Lotter, H Pircher, Steel Res. 63 (1992) 331-336.
[24] S.W. Thompson, P.R. Howell, Mater. Sci. Technol. 8 (1992) 777-784.
[25] F.G. Caballero, C. Garcia-Mateo, M.J. Santofimia, M.K. Miller, C. García de Andrés, Acta Mater. 57 (2009) 8-17.
[26] F.G. Caballero, M.K. Miller, S.S. Babu, C. Garcia-Mateo, Acta Mater. 55 (2007), 381-390.
[27] F.G. Caballero, C. García-Mateo, J. Chao, M.J. Santofimia, C. Capdevila, C. García de Andrés, ISIJ Int. 48 (2008) 1256–1262.
[28] E. Keehan, L. Karlsson, H.O. Andrén, Sci. Technol. Weld. Joining 11 (2006) 1-8.
[29] S. Chatterjee, H.K.D.H. Bhadeshia, Mater. Sci. Technol. 22 (2006) 645-649.
[30] J.H. Pak, H.K.D.H. Bhadeshia, L. Karlsson, E. Keehan, Sci. Technol. Weld. Joining 13 (2008) 593-597.
[31] E. Keehan, L. Karlsson, H.K.D.H. Bhadeshia, M. Thuvander, Mater. Sci. Technol. 24 (2008) 1183-1188.
[32] G. Avramovic-Cingara, Y. Ososkov, M.K. Jain, D.S. Wilkinson, Mater. Sci. Eng. doi: 10.1016/j.msea.2009.03.055.
[33] F.G. Caballero, A. Garcia-Junceda, C. Capdevila, C. García de Andrés, Mater. Trans. 47 (2006) 2269-2276.

Table Captions:

Table 1. Chemical Composition, [wt-%].

Table 2. Quantitative Data on Microstructure and Hardness.

Table 3. Tensile and Charpy Impact Test Results.

Table 4. Driving force for bainite formation at 500 ºC in the studied steels.

Table 5. Characterisation of martensite bands in hot rolled bainitic steels

Figure Captions:

Fig. 1. LOM micrographs of the bainitic microstructure obtained in all the steels by air cooling from ~500ºC after an initial accelerating cooling: (a) CENIM 1, (b) CENIM 2, (c) CENIM 3, (d) CENIM 4, (e) CENIM 5, and (f) CENIM 6. Longitudinal samples.

Fig. 2. SEM micrographs of the bainitic microstructure obtained in all the steels by air cooling from ~500ºC after an initial accelerating cooling: (a) CENIM 1, (b) CENIM 2, (c) CENIM 3, (d) CENIM 4, (e) CENIM 5, and (f) CENIM 6.

Fig. 3. TEM micrographs of the bainitic microstructure obtained in all the steels by air cooling from ~500ºC after an initial accelerating cooling: (a) CENIM 1, (b) CENIM 2, (c) CENIM 3, (d) CENIM 4, (e) CENIM 5, and (f) CENIM 6.

Fig. 4. Charpy impact results as a function of (a) the volume fraction of bainitic ferrite and (b) martensite.

Fig. 5. Charpy impact results as a function of (a) the volume fraction of martensite in bands and (b) inside bainite sheaves. Open symbol indicates CENIM 6 sample with a remarkable deterioration in toughness.

Fig. 6.- SEM micrographs of (a) CENIM 5 and (b) CENIM 6 steels illustrating the presence of coalesced bainite (CB).

Fig. 7. TEM micrographs in CENIM 6 steel illustrating carbide precipitation inside coalesced bainite.

Fig. 8.- Vickers microhardness values of (a) CENIM 3 and (b) CENIM 6 steels illustrating the heterogeneous hardness distribution associated to microstructural banding.

Fig. 9. Fractographs of CENIM 6 steel impact specimen at -40 ºC: (a) Macrograph of fracture surface, (b) SEM fractograph of a region close to the notch, (c) enlarge region of zone A and (d) enlarge region of zone B.

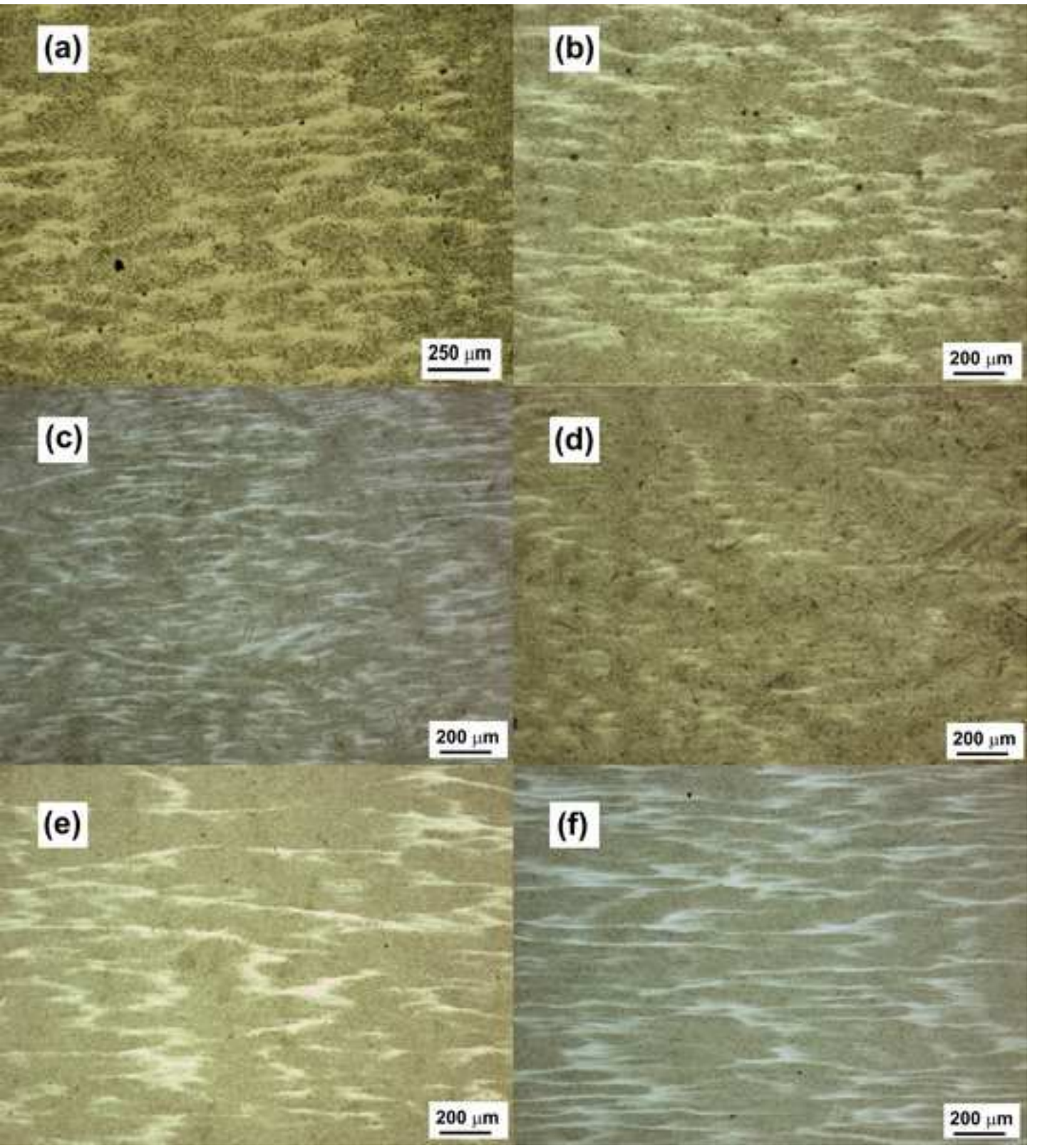
(a)
250 μm
(b)
200 μm
(c)
200 μm
(d)
200 μm
(e)
200 μm
(f)
200 μm

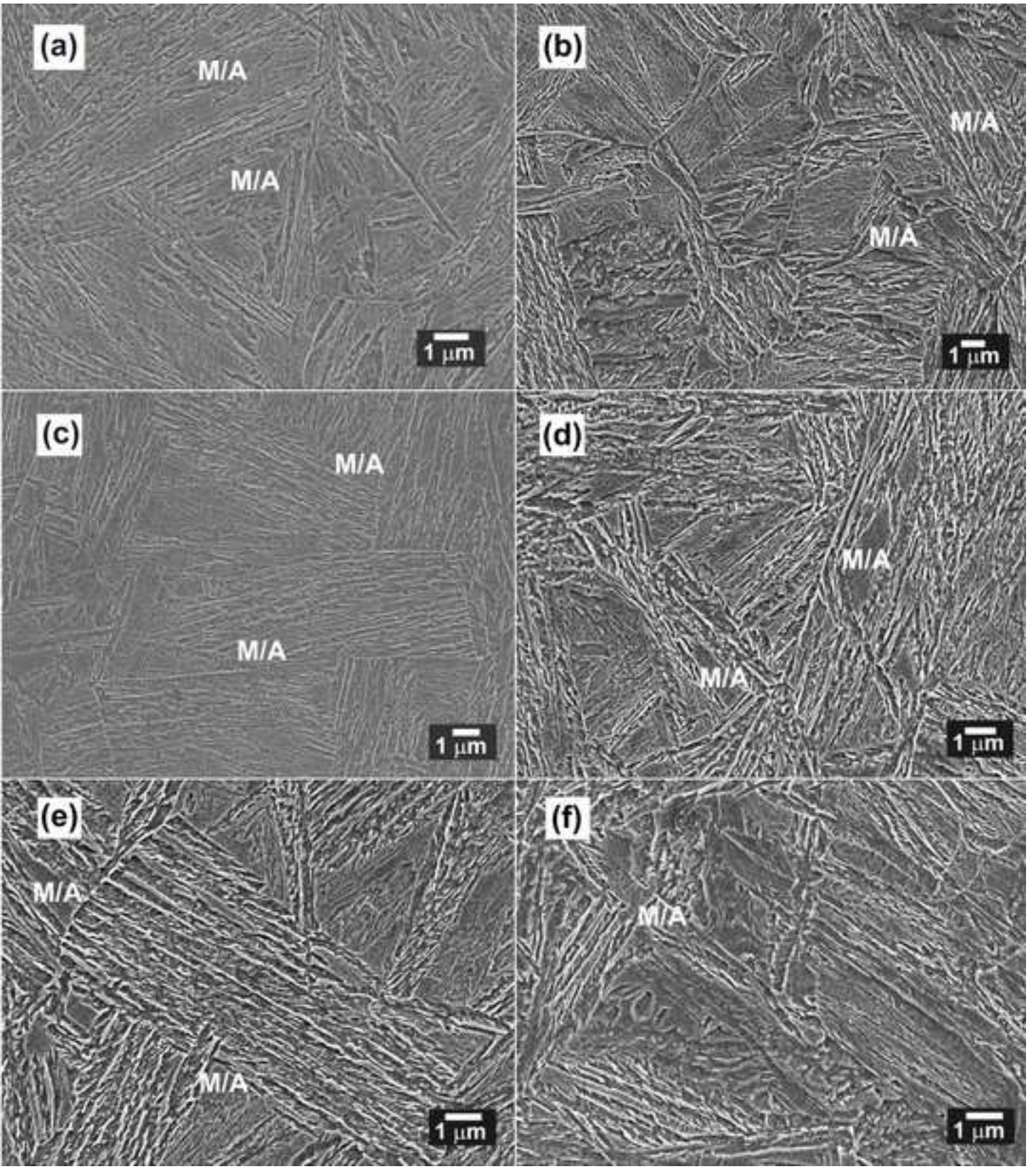
(a)
M/A
M/A
1 μm
(b)
M/A
M/A
1 μm
(c)
M/A
M/A
1 μm
(d)
M/A
M/A
1 μm
(e)
M/A
M/A
1 μm
(f)
M/A
1 μm

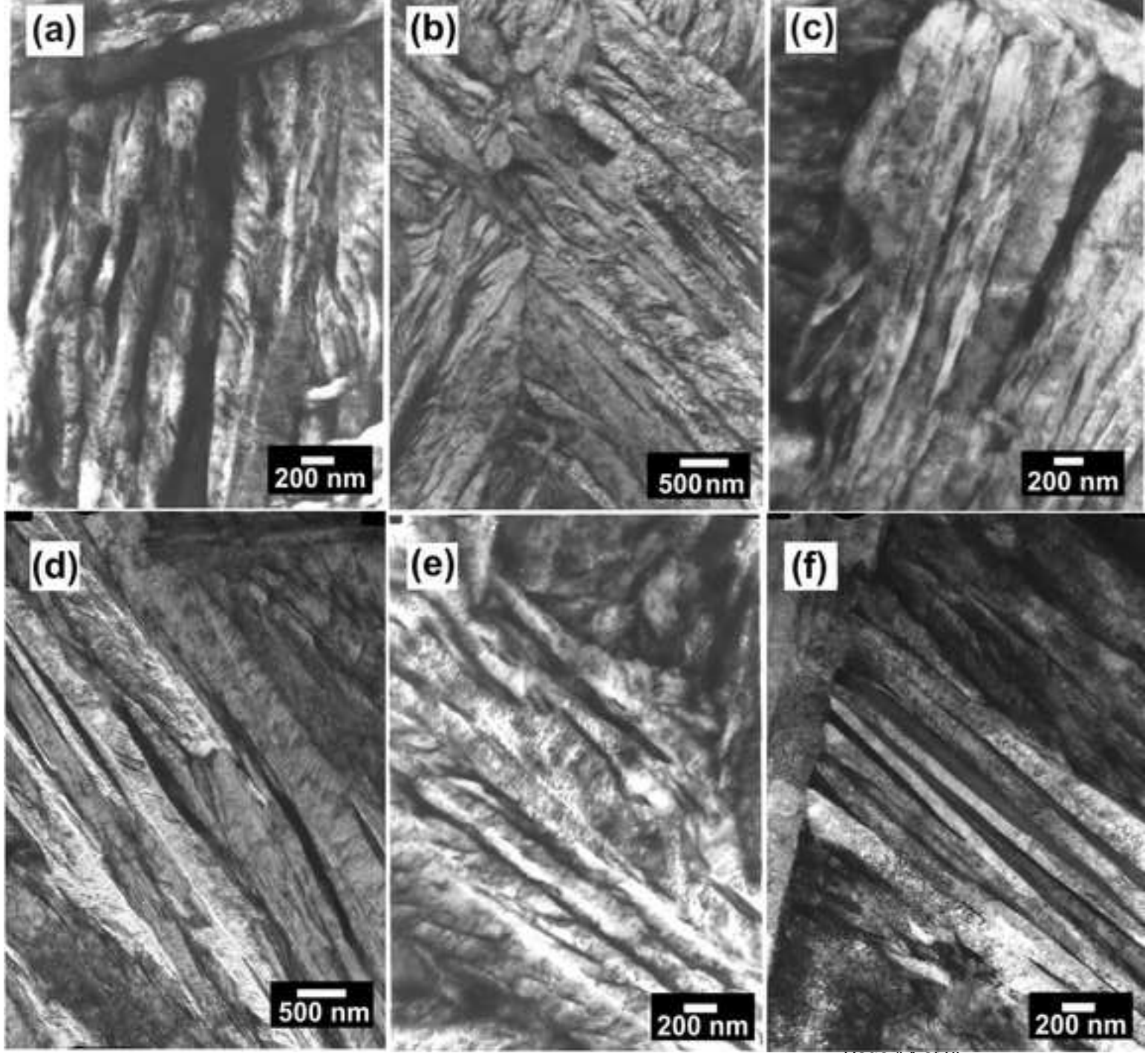
(a)
200 nm
(b)
500 nm
(c)
200 nm
(d)
500 nm
(e)
200 nm
(f)
200 nm

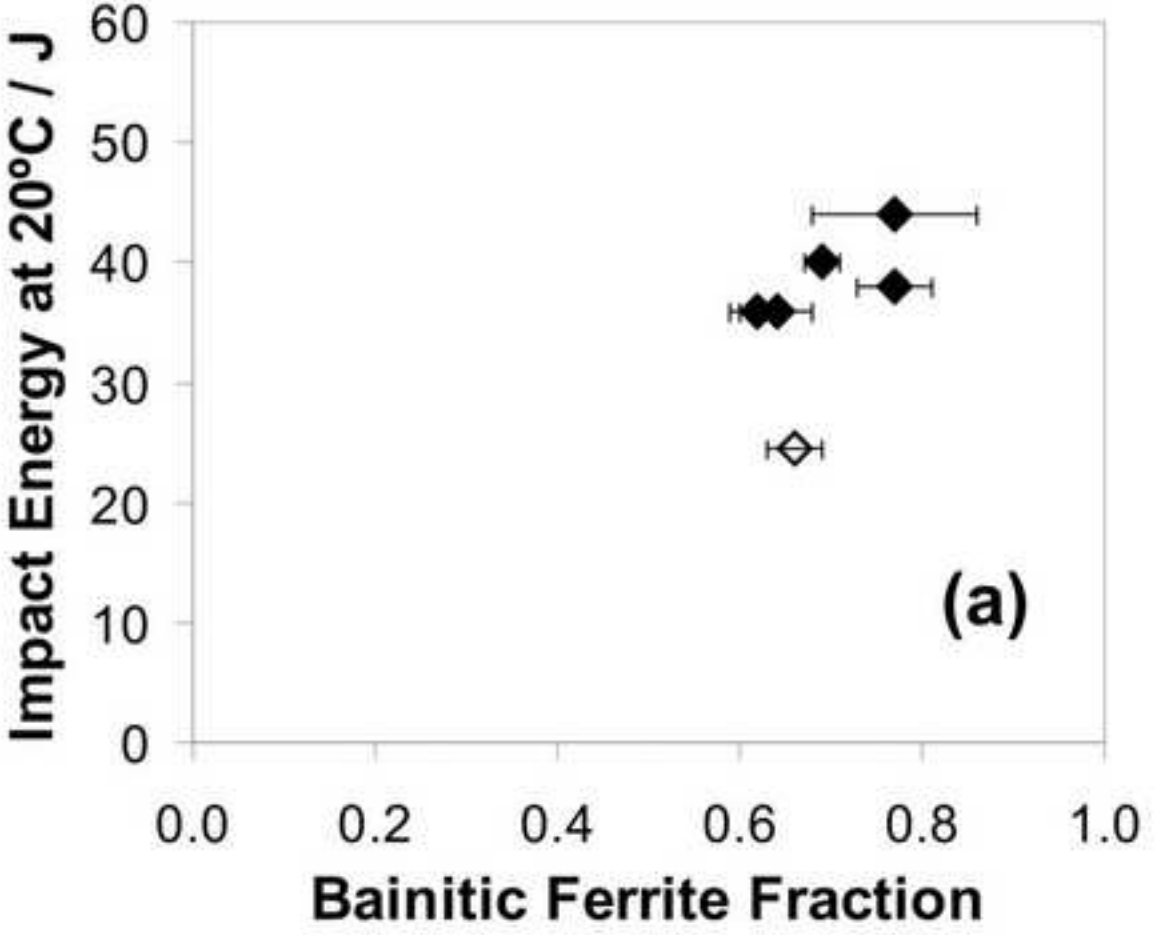
Impact Energy at 20°C / J
60
50
40
30
20
10
0
0.0
0.2
0.4
0.6
0.8
1.0
Bainitic Ferrite Fraction
(a)

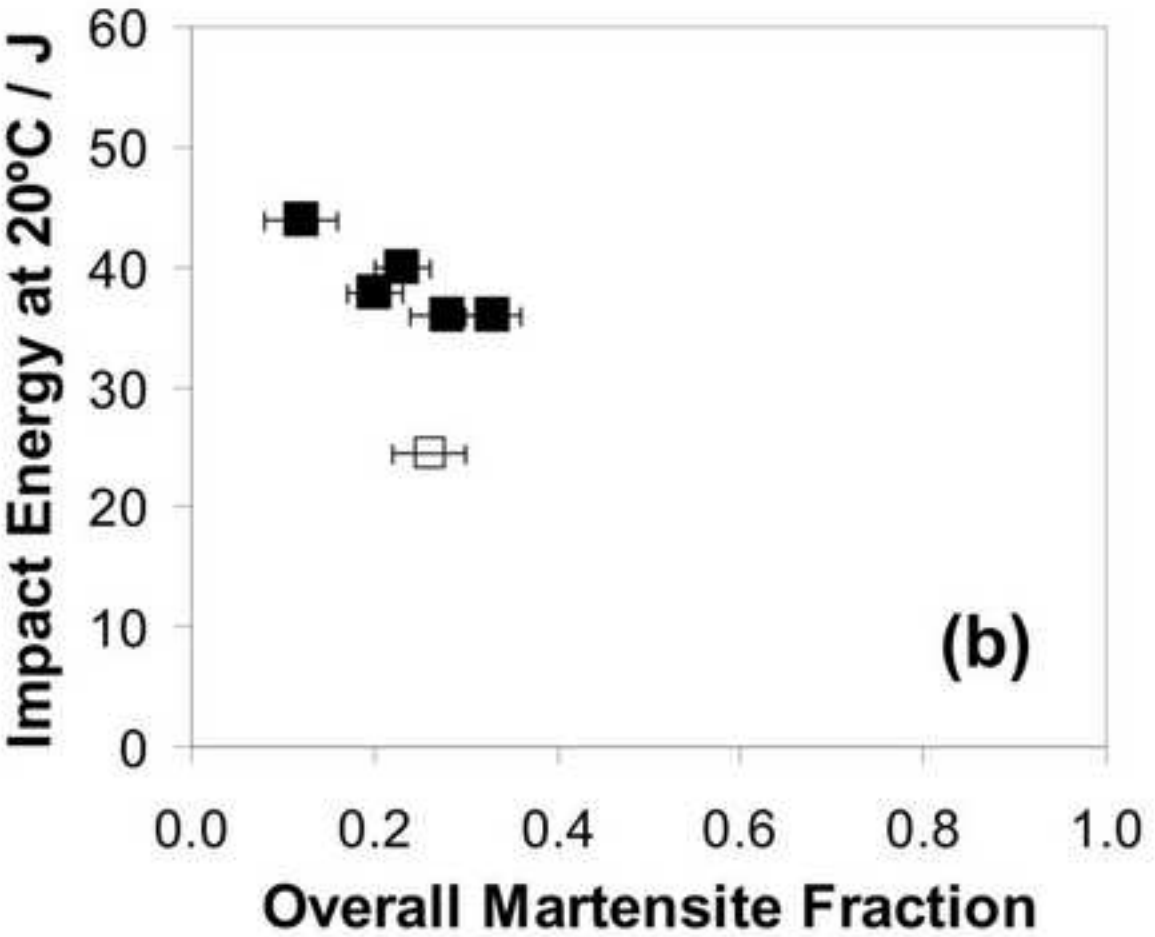
Impact Energy at 20°C / J
60
50
40
30
20
10
0
0.0
0.2
0.4
0.6
0.8
1.0
Overall Martensite Fraction
(b)

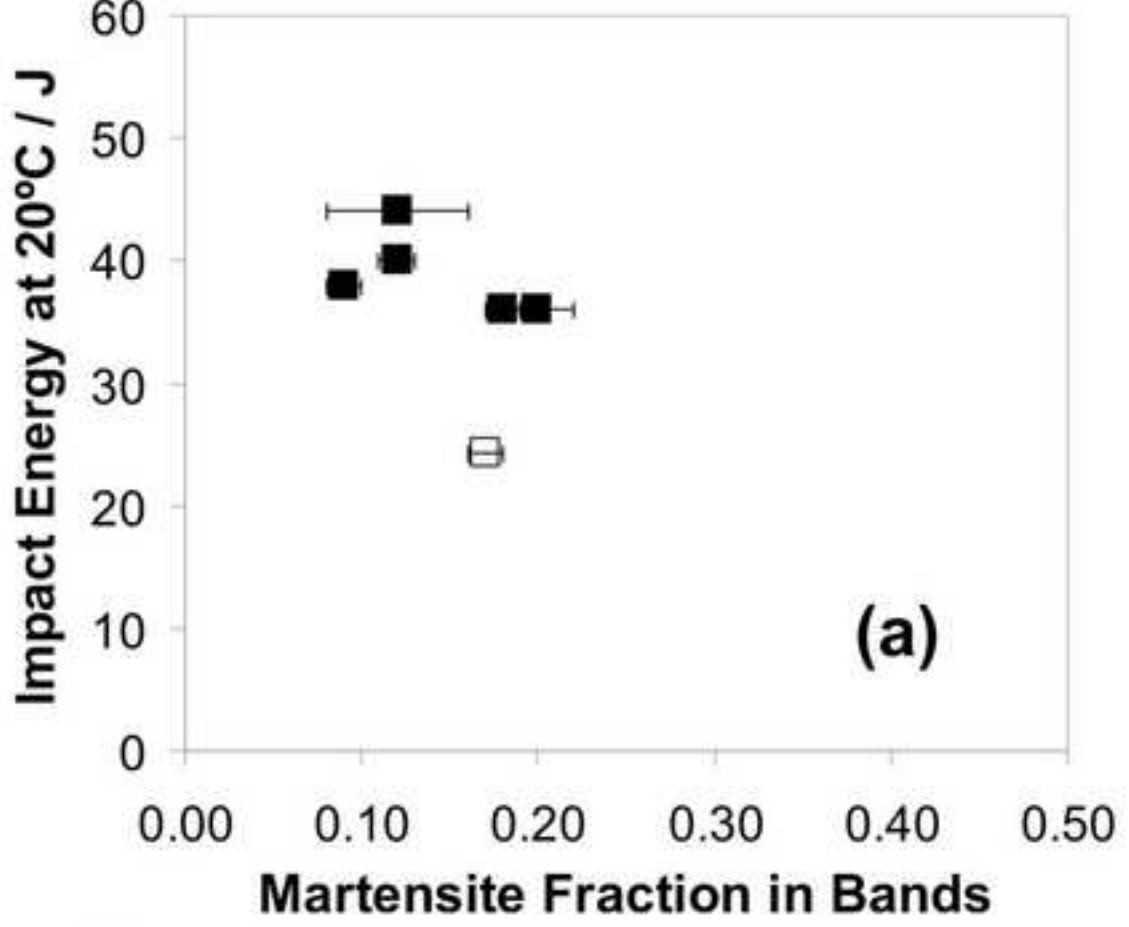
Impact Energy at 20°C / J
60
50
40
30
20
10
0
0.00
0.10
0.20
0.30
0.40
0.50
Martensite Fraction in Bands
(a)

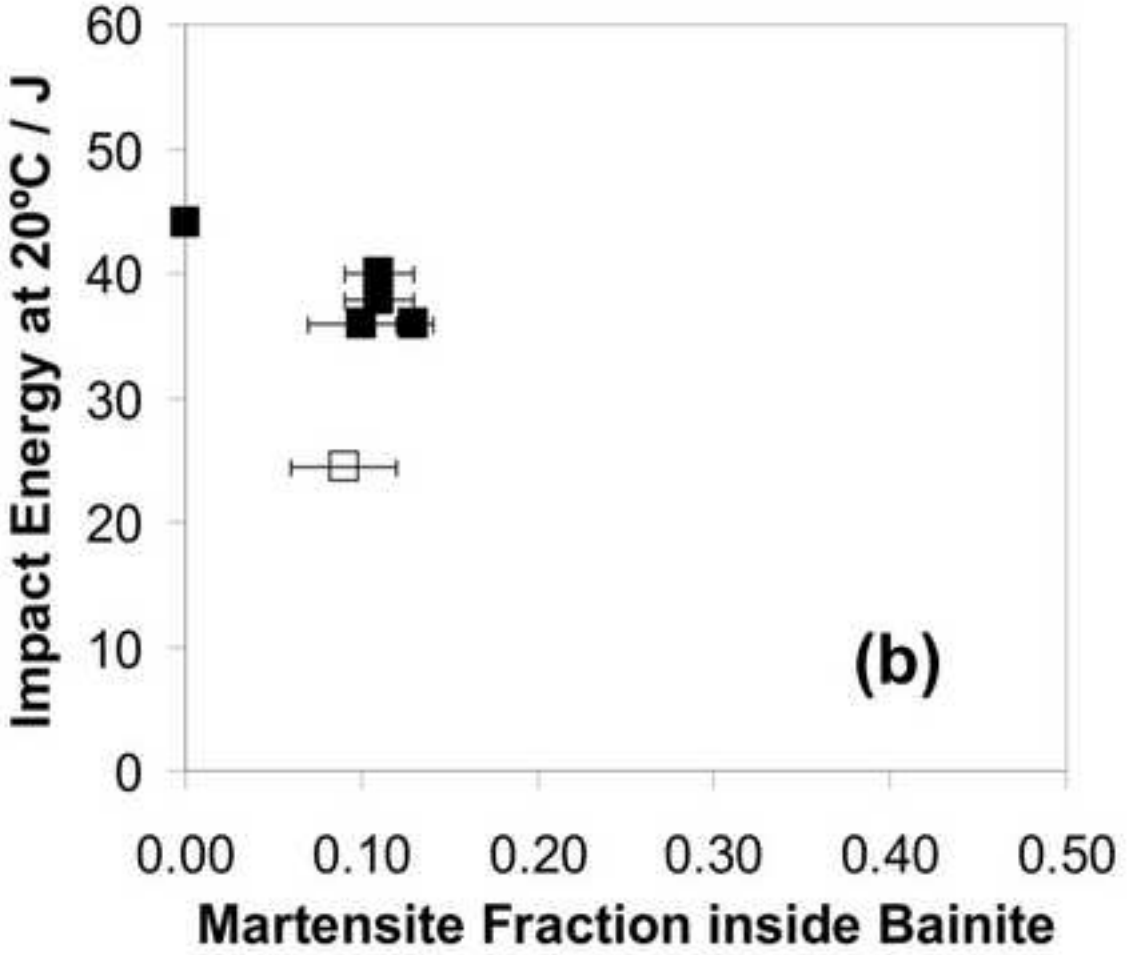
Impact Energy at 20°C / J
60
50
40
30
20
10
0
0.00
0.10
0.20
0.30
0.40
0.50
Martensite Fraction inside Bainite
(b)

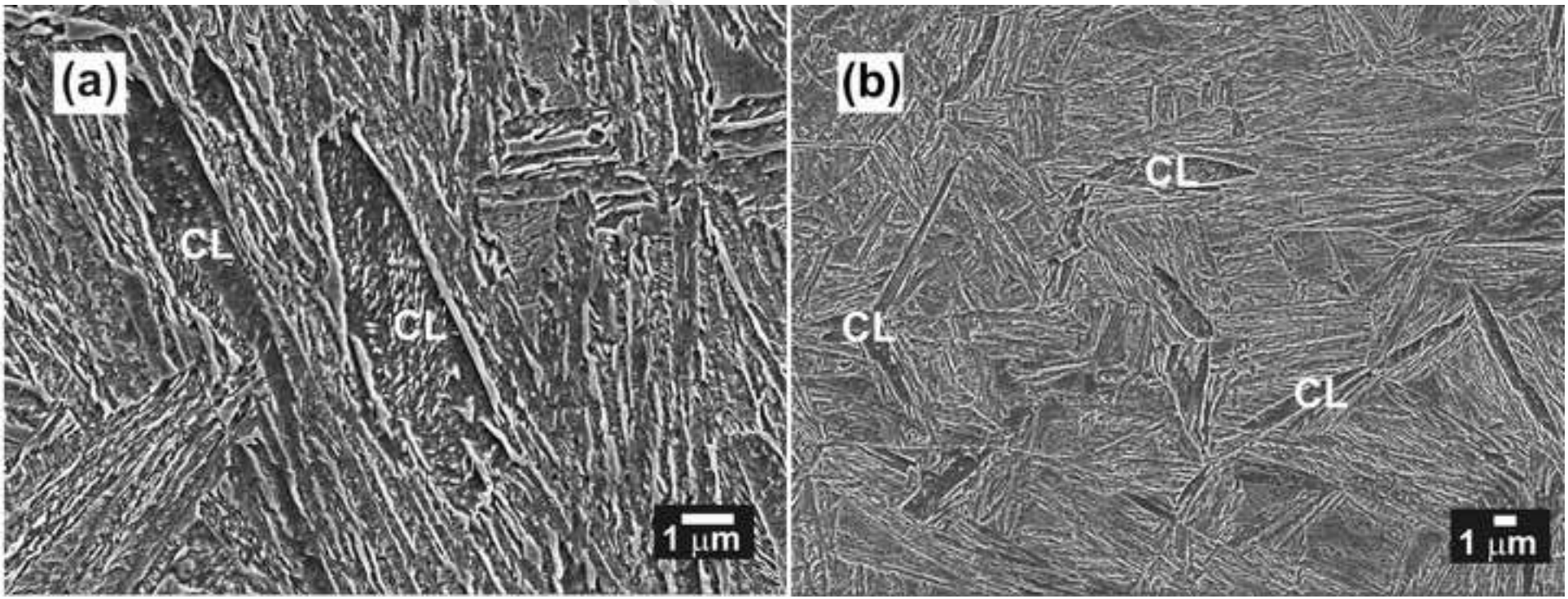
(a)
CL
CL
1 μm
(b)
CL
CL
CL
1 μm

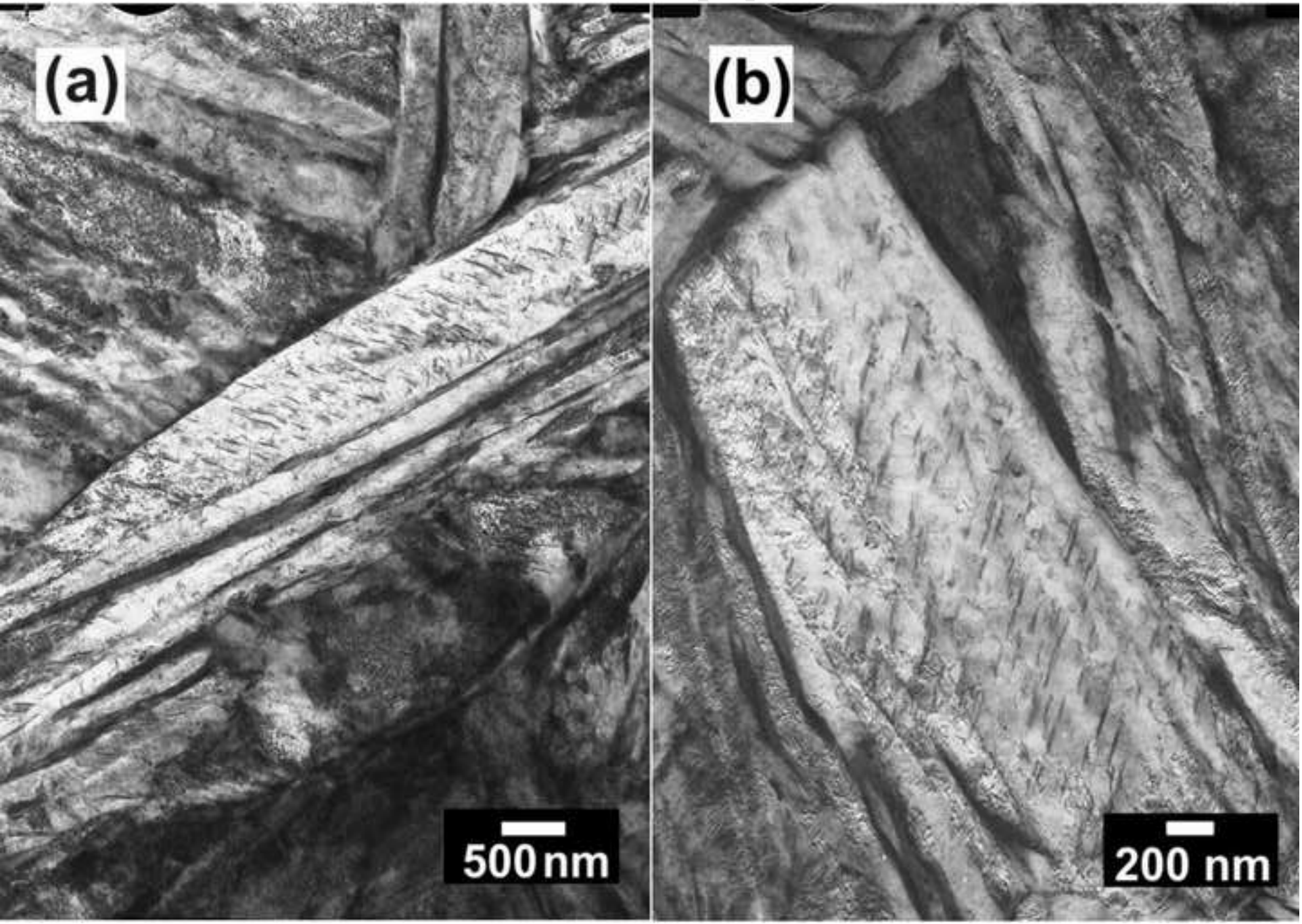
(a)
500 nm
(b)
200 nm

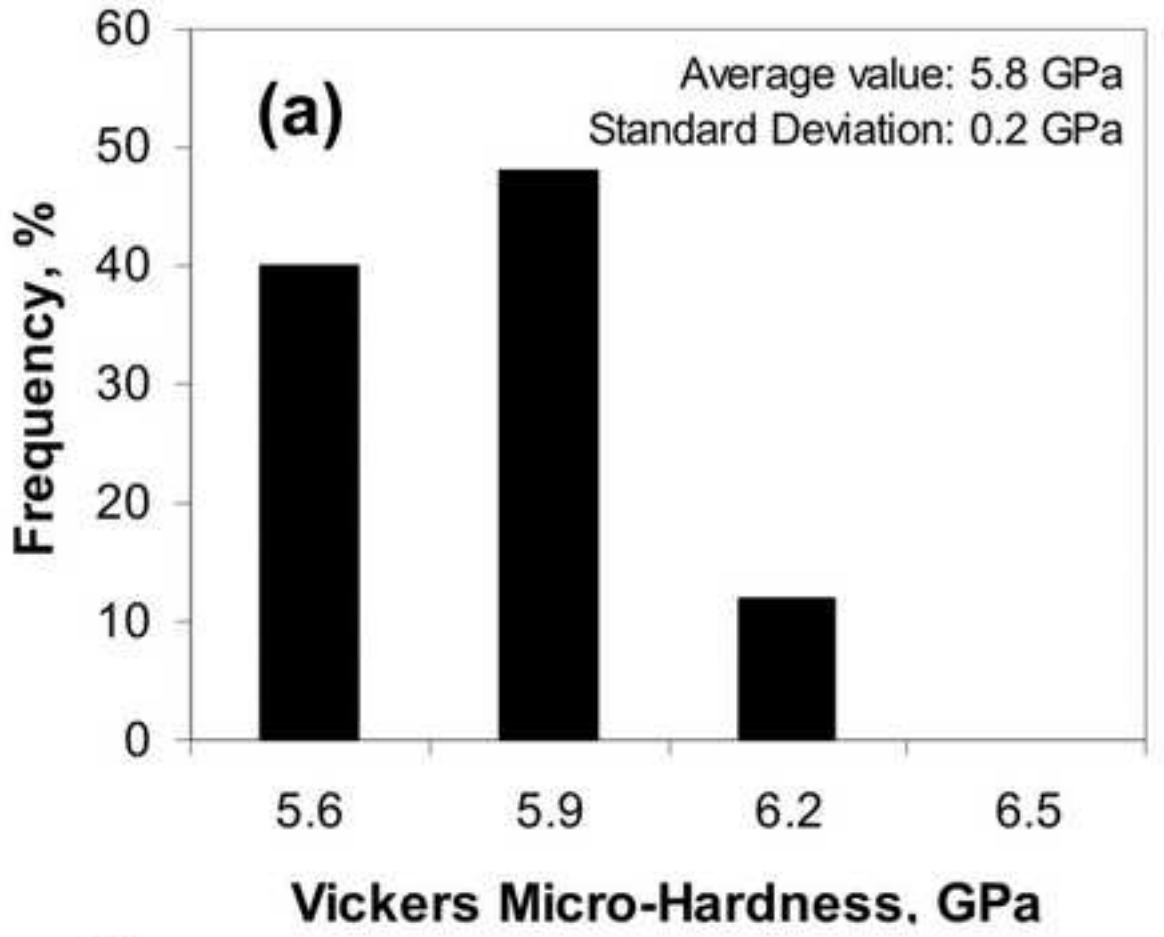
(a)
Average value: 5.8 GPa
Standard Deviation: 0.2 GPa
Frequency, %
60
50
40
30
20
10
0
5.6
5.9
6.2
6.5
Vickers Micro-Hardness, GPa

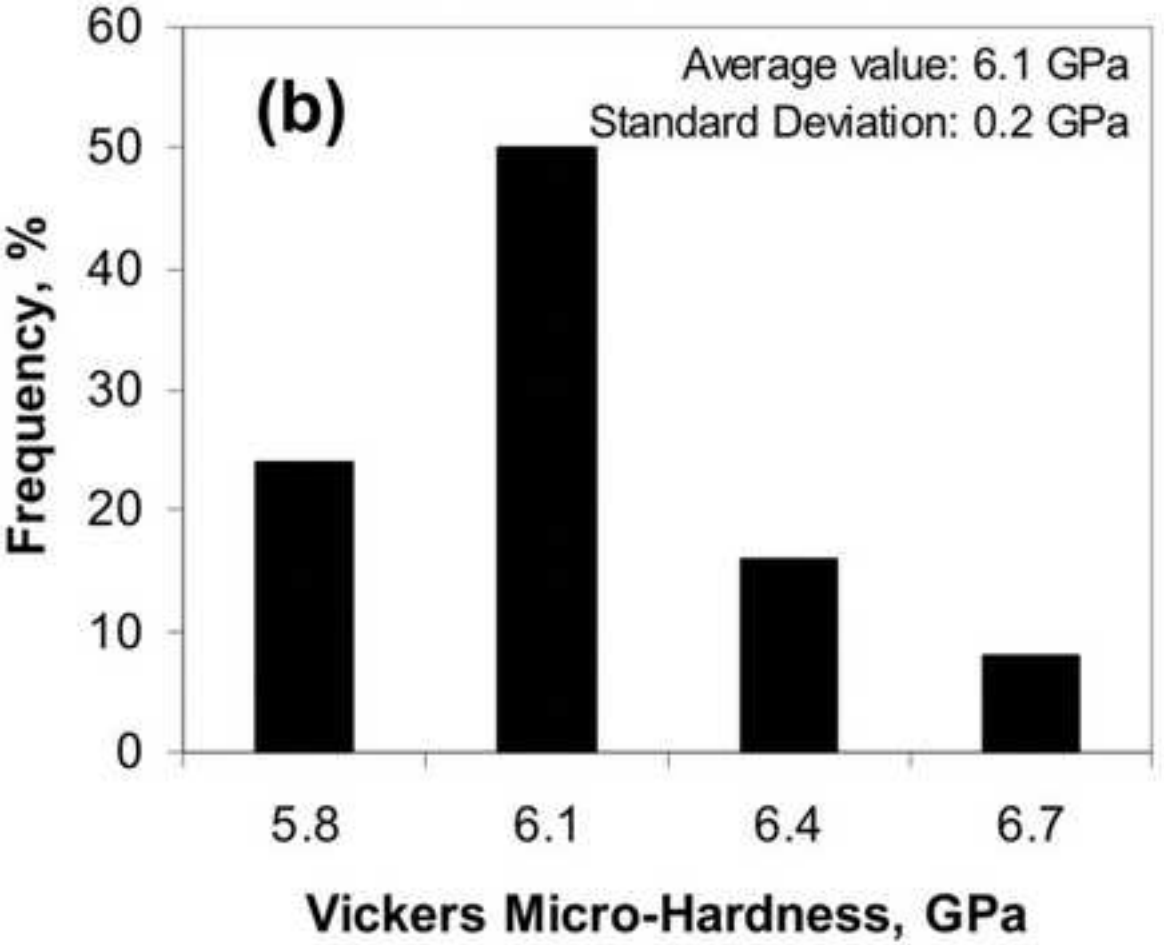
(b)
Average value: 6.1 GPa
Standard Deviation: 0.2 GPa
Frequency, %
60
50
40
30
20
10
0
5.8
6.1
6.4
6.7
Vickers Micro-Hardness, GPa

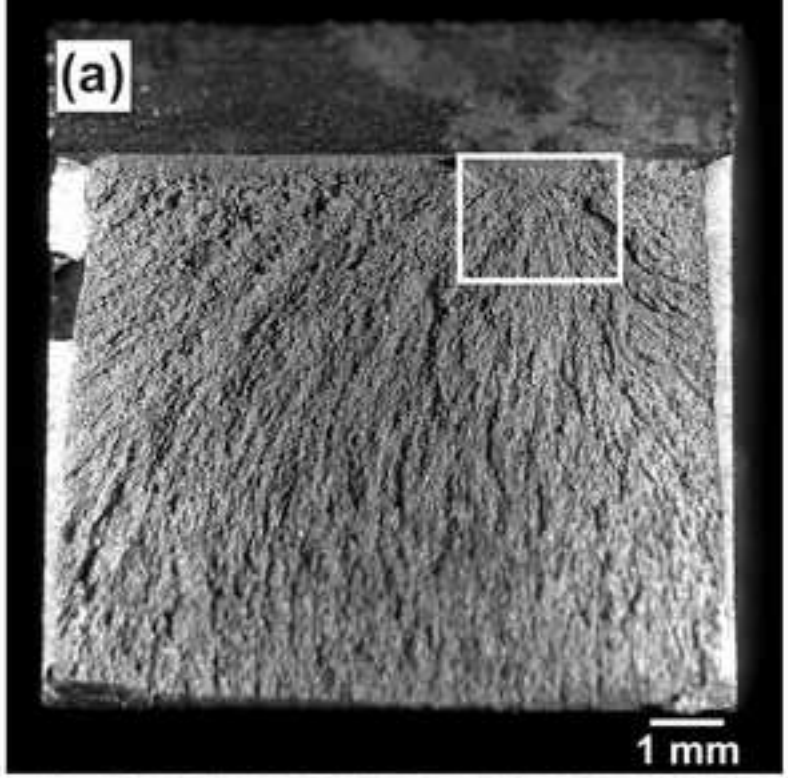
(a)
1 mm

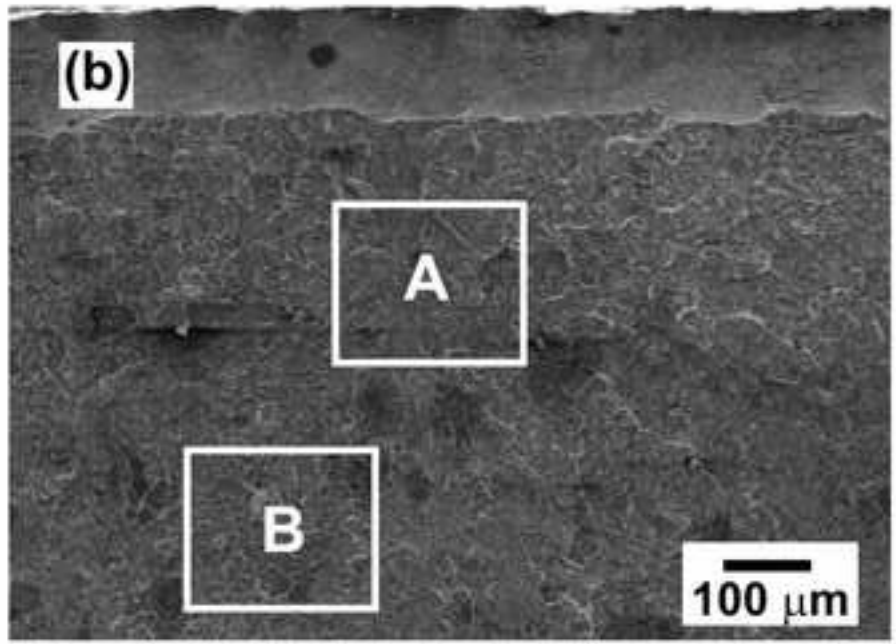
(b)
A
B
100 μm

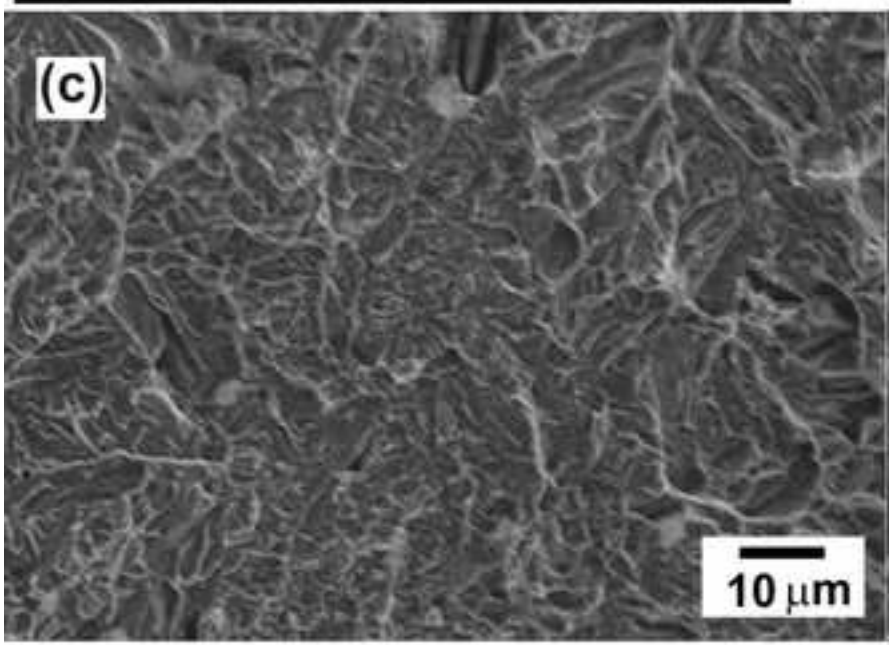
(c)
10 μm

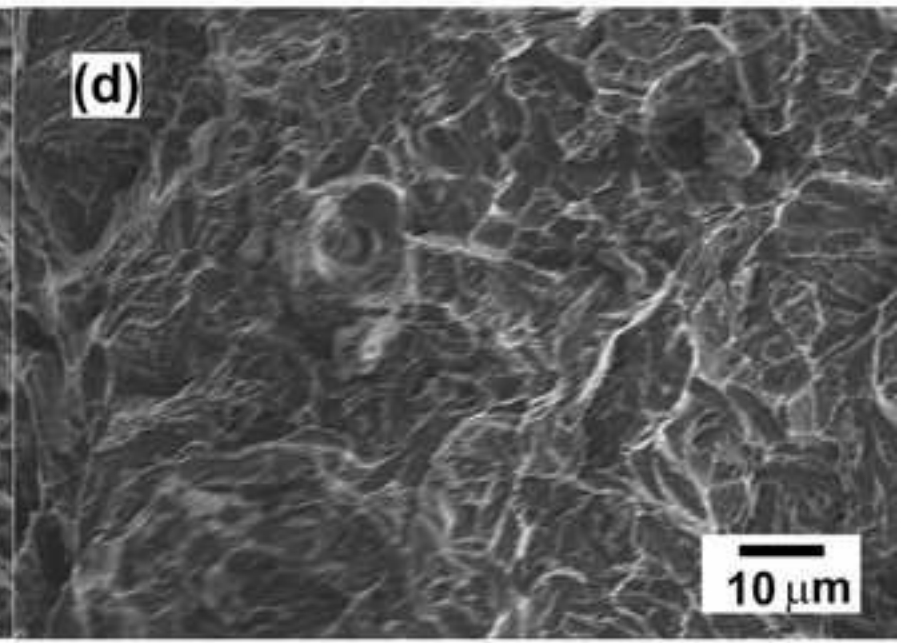
(d)
10 μm

Table 1. Chemical Composition, [wt-%]

Steel	C	Si	Mn	Ni	Cr	Mo	Co
CENIM 1	0.29	1.50	2.25	---	---	0.26	---
CENIM 2	0.29	1.46	1.97	---	0.46	0.25	---
CENIM 3	0.29	1.49	1.56	---	1.47	0.25	---
CENIM 4	0.27	1.71	1.53	1.47	0.17	0.24	---
CENIM 5	0.29	1.47	1.97	---	1.20	0.25	0.97
CENIM 6	0.28	1.50	2.04	---	1.50	0.24	1.48

Table 2. Quantitative Data on Microstructure and Hardness

Steel	$V_{\alpha b}$	$V_{M\ in\ bands}$	$V_{M\ in\ bainite}$	V_{γ}	x_{γ} [wt-%]	Hardness HV30
CENIM 1	0.64 ± 0.04	0.20 ± 0.02	0.13 ± 0.01	0.03 ± 0.01	0.72 ± 0.06	530 ± 7
CENIM 2	0.62 ± 0.03	0.18 ± 0.01	0.10 ± 0.03	0.10 ± 0.01	1.18 ± 0.03	519 ± 3
CENIM 3	0.77 ± 0.09	0.12 ± 0.08	---	0.11 ± 0.01	1.07 ± 0.05	495 ± 15
CENIM 4	0.77 ± 0.04	0.09 ± 0.01	0.11 ± 0.04	0.03 ± 0.01	1.29 ± 0.07	531 ± 10
CENIM 5	0.69 ± 0.02	0.12 ± 0.01	0.11 ± 0.02	0.08 ± 0.01	1.22 ± 0.07	521 ± 12
CENIM 6	0.66 ± 0.03	0.17 ± 0.01	0.09 ± 0.03	0.08 ± 0.01	1.68 ± 0.30	555 ± 14

$V_{\alpha b}$ is the volume fraction of bainitic ferrite ($V_{\alpha b}=1-V_{M\ in\ bands}-V_{M\ in\ bainite}-V_{\gamma}$); $V_{M\ in\ bands}$ is the volume fraction of martensite in bands; $V_{M\ in\ bainite}$ is the volume fraction of martensite inside bainite sheaves; V_{γ} is the volume fraction of retained austenite; x_{γ} is the carbon content in retained austenite

Table 3. Tensile and Charpy Impact Test Results.

Steel	YS [MPa]	UTS [MPa]	Impact Energy [J]						
			-40 ºC	-20ºC	0ºC	20ºC	50ºC	100ºC	150ºC
CENIM 1	1240±31	1796±21	---	---	29	36	---	42	38
CENIM 2	1187±16	1606±30	---	---	---	36	39	55	55
CENIM 3	1194±35	1652±6	---	32	39	44	---	61	61
CENIM 4	1339±16	1763±18	30	---	---	38	47	50	---
CENIM 5	1232±4	1701±16	---	---	---	40	40	65	56
CENIM 6	1448±32	1854±4	19	---	---	24	32	35	---

Table 4. Driving force for bainite formation at 500 ºC in the studied steels

Steel	$\Delta G^{\gamma\alpha}$ [J mol^{-1}]
CENIM 1	-689
CENIM 2	-727
CENIM 3	-786
CENIM 4	-670
CENIM 5	-778
CENIM 6	-813

Table 5. Characterisation of martensite bands in hot rolled bainitic steels

Steel	$V_{M\ in\ bands}$	AI	λ [μm]
CENIM 1	0.20 ± 0.02	1.2 ± 0.1	72 ± 2
CENIM 2	0.18 ± 0.01	2.4 ± 0.7	94 ± 1
CENIM 3	0.12 ± 0.08	3.2 ± 0.3	72 ± 9
CENIM 4	0.09 ± 0.01	1.7 ± 0.2	136 ± 9
CENIM 5	0.12 ± 0.01	2.6 ± 0.3	82 ± 1
CENIM 6	0.17 ± 0.01	9.8 ± 0.3	32 ± 1

$V_{M\ in\ bands}$ is the volume fraction of martensite in bands; AI is anisotropy index; λ is the mean edge-to-edge spacing of the bands